Resonance polarization and phase-mismatched CARS of pheophytinb excited in theQy band

ARTICLE *in* JOURNAL OF RAMAN SPECTROSCOPY · JUNE 1993

Impact Factor: 2.67 · DOI: 10.1002/jrs.1250240608

4 AUTHORS, INCLUDING:

Gerald Lucassen
Philips
69 PUBLICATIONS **1,782** CITATIONS
SEE PROFILE

Cees Otto
University of Twente
231 PUBLICATIONS **5,255** CITATIONS
SEE PROFILE

Jan Greve
University of Twente
304 PUBLICATIONS **8,801** CITATIONS
SEE PROFILE

JOURNAL OF RAMAN SPECTROSCOPY, VOL. 24, 383–396 (1993)

Resonance Polarization and Phase-Mismatched CARS of Pheophytin *b* Excited in the Q_y Band

W. P. de Boeij, G. W. Lucassen, C. Otto and J. Greve*
Applied Optica Group, Department of Applied Physics, University of Twente, P.O. Box 217, 7500 AE Enschede, The Netherlands

Resonance polarization and phase-mismatched coherent anti-Stokes Raman scattering (CARS) measurements were performed on pheophytin *b* dissolved in acetone excited in the Q_y absorption band, where strong broad fluorescence makes spontaneous Raman spectroscopy impossible. The phase-mismatching technique was applied to suppress solvent background and used in combination with the polarization-sensitive CARS technique to measure directly the $\chi^{(3)}_{1111}$ and $\chi^{(3)}_{1221}$ components to estimate depolarization ratios. The spectra were fitted by a non-linear least-squares procedure yielding vibrational band parameters. Some CARS dispersion information on the vibrational amplitudes was obtained by varying the pump wavelength. CARS excitation profiles based on transform theory were calculated and partly explain the observed amplitude dispersion. The application of the combined phase-mismatched polarization CARS technique may be useful in many other cases of highly fluorescing molecules when resonantly excited.

INTRODUCTION

Pheophytins are extraction products of chlorophylls, which are the characteristic pigments of photosynthetic organisms that play an important role in the process of light absorption, energy and electron transfer in higher plants and many algae.[1] Numerous studies (x-ray crystallography, visible, infrared and fluorescence spectroscopy) on chlorophylls have been carried out to elucidate their spectroscopic properties.[1–4] Since 1972, resonance spontaneous Raman scattering (RS) studies, started by Lutz,[5] have yielded an enormous amount of information on the conformation, electronic structure and function of the chlorophyll molecule.

The importance of the resonance RS technique in studying chlorophylls lies in its ability to probe selectively chromophores with different electronic absorptions in compounds. The photosynthetic organisms contain chlorophyll, carotenoid and phycobillin pigments, which have complementary electronic absorption bands ranging from the visible to the near-ultraviolet and can thus be probed by proper selection of the excitation wavelength. This makes application of the resonance RS techniques to chlorophyll studies *in vivo* possible, although *in vitro* studies are inevitable to assign the many (55) vibrations observed in the 50–1750 cm^{-1} spectral range.[5–7] Excitation in the higher electronic absorption bands has yielded vibrational information on the different chlorophyll and pheophytin species. However, on excitation in the lowest electronic Q_y absorption band, RS is accompanied by an intense and broad fluorescence of these molecules. So far, no RS measurements of these fluorescing molecules have been obtained with excitation in this Q_y band. Recently, Mattioli *et al.*[8] measured resonant RS spectra and Raman excitation profiles (REP) of non-luminescent Ni(II)–pheophytin *a* in benzene, excited in the Q_y absorption band.

The coherent anti-Stokes Raman scattering (CARS) technique, a non-linear optical variant of Raman spectroscopy which is insensitive to this fluorescence, enables measurements to be made of the fluorescing chlorophyll and pheophytin molecules in this region. Resonance CARS, just like RS, is electronically enhanced when the exciting frequency (and CARS signal frequency) lie in the electronic absorption bands.

In 1977 Lau *et al.*[9] used the resonance CARS technique to obtain vibrational information on chlorophylls *in vivo* and *in vitro* with excitation by a ruby laser at 694.3 nm. Several reports on resonance CARS of chlorophylls originated from this group.[10–12] In these studies no polarization information was obtained. The information obtained from CARS is essentially similar to that obtained from RS, although CARS has some advantages which follow from the different selection rules under electron resonant excitation conditions.[13]

Scholten[14] used the resonance polarization sensitive CARS (PCARS) technique to study chlorophyll *b* in ethanol excited near the centre of the Q_y absorption band at 645 nm. However, at that time lack of a proper flow cuvette made these measurements difficult since the very photolabile chlorophyll molecules were partly degraded. The present study concerns improved measurements in the high-frequency region (1100–1650 cm^{-1}) on the more stable pheophytin *b* molecule *in vitro* under resonant excitation in the Q_y absorption band. Another reason for studying the pheophytin *b* molecule instead of the chlorophyll *b* molecule lies in the fact that on excitation in the Q_y band the spectral information from the former is comparable to that of the latter, in spite of the difference in molecular structure caused by an Mg atom in the centre being replaced by two H atoms. Further, most vibrations in which the Mg atom is involved are observed in the low-frequency

* Author to whom correspondence should be addressed.

0377-0486/93/060383-14 $12.00

Received 9 November 1992
Accepted 10 February 1993

region ($< 1000\ cm^{-1}$), in particular when excited in the Soret absorption band at higher energy.

In the work presented here the phase-mismatching CARS (PMM-CARS) technique, previously reported,[15–17] was used in combination with PCARS to measure the $\chi^{(3)}_{1111}$ and $\chi^{(3)}_{1221}$ components of the third-order non-linear susceptibility. In addition, dispersion information was obtained by measuring the $\chi^{(3)}_{1111}$ component at various excitation wavelengths in the 630–645 nm range. Spectral analysis was carried out by curve fitting the CARS line shapes using a non-linear least-squares procedure.

It is shown that under these excitation conditions an unexpected, anomalously polarized band at 1575 cm^{-1} is obtained and that the amplitude dispersions of various bands behave differently. This dispersion can partly be explained from a simple model based on transform theory of CARS excitation profiles (CEP) including vibronic coupling similar to calculation of Raman excitation profiles reported in Ref. 8. We shall show that combined phase-mismatched and polarization CARS measurements provide the unique possibility of measuring polarization and dispersion characteristics of the highly fluorescing pheophytin molecules excited in the lowest electronic Q_y band. These are inaccessible to the spontaneous Raman technique.

In this paper we discuss briefly the PCARS and PMM-CARS techniques, the fitting procedure used and theory of CARS excitation profiles. The experimental details of the sample, set-up and measurements are given. The results of measurements, fit analyses and discussion follow. Finally, we comment on the results and possibilities of these CARS techniques in the study of photosynthetic systems. A short theory of PCARS and PMM-CARS is given in Appendices A and B; more details can be found in the references cited.

THEORY

PCARS and PMM-CARS

The single degenerate CARS method uses two laser beams, one with a fixed frequency ω_p (pump beam) and one with variable-frequency ω_s (Stokes beam). The two incident linearly polarized electric fields $\mathbf{E}_{p,s}$ with polarization vectors $\mathbf{e}_{p,s}$ and frequencies $\omega_{p,s}$ induce a third-order polarization $\mathbf{P}^{(3)}$ in the medium, which generates the nonlinear CARS signal at frequency ω_a, arising from non-resonant and vibration resonant processes:

$$\mathbf{P}^{(3)} = \mathbf{P}^{(3)NR} + \mathbf{P}^{(3)R} = [\chi^{(3)NR} + \chi^{(3)R}]\mathbf{E}_p\,\mathbf{E}_p\,\mathbf{E}_s^* \quad (1)$$

The non-resonant part of the third-order susceptibility $\chi^{(3)NR}$ often has negligible dispersion in the spectral range considered and can be taken as a real constant. The resonant third-order susceptibility $\chi^{(3)R}$ can be written as

$$\chi^{(3)R} = \sum_t \frac{A_t^R \exp(i\theta_t^R)}{-i + \Delta_t} \quad (2)$$

where the complex numerator with amplitude A_t^R and phase θ_t^R contains the dependence on electronic transitions, with resonances at ω_p and ω_a, and orientational averaged direction cosines between the transition dipole moments in the molecule and the applied electric field polarizations. The denominator contains the Raman vibrational part with the bandwidth-normalized, frequency detuning $\Delta_t = [\Omega_t - (\omega_p - \omega_s)]/\Gamma_t$, where the difference $\omega_p - \omega_s$ is scanned across the Raman resonances Ω_t. The summation over t involves all Raman resonances. The correspondence between spontaneous Raman and CARS is that the RS intensity is proportional to the imaginary part of $\chi^{(3)R}$.

Detecting the polarization CARS (PCARS) signal with an analyser $\mathbf{e}_A$, the measured PCARS intensity $I_A(\omega_a)$ can be written as

$$I_A(\omega_a) \sim |(\mathbf{e}_A^* \cdot \chi^{(3)}(\omega_a)\mathbf{e}_p\,\mathbf{e}_p\,\mathbf{e}_s^*)|^2 \times I_p^2 I_s M(\Delta k, L) \quad (3)$$

where the components of $\chi^{(3)}$ will be written $\xi^{(3)}_{Apps}$ with the subscripts Apps corresponding to analyser, pump and Stokes field polarizations, I_p and I_s are the incident pump and Stokes beam intensities, $(M(\Delta k, L)$ is a phase-matching factor which in general depends on the (complex) wave vectors and the overlap length L of the beams in the medium. In dispersive condensed media such as liquids, phase matching is achieved by crossing the beams in the sample at an angle η, and collection of the CARS signal is obtained at an angle ν with respect to the optical axis, which coincides with the pump beam direction.

Generally, when using linear polarizations of the input beams, the vibration resonant polarization vector $\mathbf{P}^{(3)R}$ and the non-resonant polarization vector $\mathbf{P}^{(3)NR}$ have different orientations (see Fig. 1 and Appendix A), which offers the possibility of suppressing the non-resonant signal by setting the analyser orientation perpendicular to $\mathbf{P}^{(3)NR}$.

In isotropic solvents, full suppression of the non-resonant polarization is achieved at angles $\psi_0 = \arctan(3/\tan\varphi)$, where φ is the angle between the pump and the Stokes polarization vectors. The projection of the vibration resonant polarization on the analyser orientation is transmitted as a (background-free) signal. By rotation of the analyser ε around the angle ψ_0 of best background suppression, the vibration resonant signal is 'heterodyned' with a (controlled) amount of

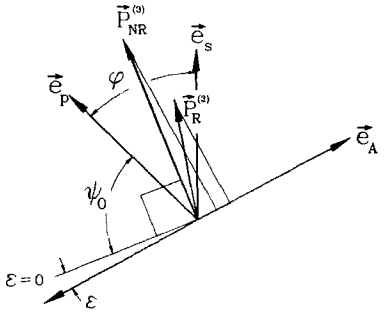

Figure 1. Polarization vector configuration in the PCARS scheme. With the angle φ between unit polarization vectors $\mathbf{e}_p$ and $\mathbf{e}_s$, the resulting vibration resonant polarization $\mathbf{P}^{(3)R}$ and $\mathbf{P}^{(3)NR}$ generally have different orientations. Non-resonant background suppression is obtained with analyser setting $\mathbf{e}_a$ perpendicular to $\mathbf{P}^{(3)NR}$. Heterodyning the resonant signal with a controlled amount of non-resonant signal is achieved by small offsets ε of the analyser orientation with respect to the orientation of full suppression.

non-resonant signal, thereby enhancing the resonant signal with non-resonant background signal. The disadvantage of the polarization-sensitive CARS technique is that for bands with polarization vectors $\mathbf{P}^{(3)R}$ closely directed along the non-resonant polarization vector $\mathbf{P}^{(3)NR}$, the suppression of the non-resonant background is accompanied by a simultaneous suppression of resonant signal. This means that bands with vibration resonant depolarization ratio $\rho^R = \chi^{(3)R}_{1221}/\chi^{(3)R}_{1111}$ close to the non-resonant one $\rho^{NR} = \chi^{(3)NR}_{1221}/\chi^{(3)NR}_{1111} = 1/3$ (in the isotropic case) are also suppressed.[18] This problem is circumvented by the phase-mismatching technique.

The PMM-CARS technique[14–17] uses coherent cancellation to suppress the non-resonant background. When using a cuvette consisting of glass windows (length L_G) surrounding the sample layer (length L_s), the non-resonant signal is built up from these three layers (in the sample layer the non-resonant signal arises mainly from the solvent), while the vibration resonant signal is built up from the sample layer only (see Fig. 2).

The dependence of the CARS signal intensity I on the phase-mismatching factor is given by[20]

$$I \sim |\chi^{(3)}|^2 I_p^2 I_s e^{-(\Delta\alpha + \alpha_a)L} \times \left[\frac{\sinh(\Delta\alpha L/2) + \sin(\Delta\beta L/2)}{(\Delta\alpha L/2)^2 + (\Delta\beta L/2)^2}\right] L^2 \quad (4)$$

where $\Delta\alpha = (2\alpha_p + \alpha_s - \alpha_a)/2$ with $\alpha_j = 2k_j''$ the exponential absorption coefficient and $\Delta\beta = n_a(\omega_a)\omega_a/c - |2\mathbf{k}_p' - \mathbf{k}_s'| = n_a(\omega_a)\omega_a/c - [4k_p'^2 + k_s'^2 - 4\cos\eta k_p' k_s']^{1/2}$ with $\beta_j = k_j' = n_j(\omega_j)/c$ the real part of the wave vector, $n_j(\omega_j)$ the refractive index at frequency ω_j (j = p, s, a) and c the velocity of light in vacuum, and η the crossing angle of the pump and Stokes beam in the sample. In the absence of absorption, i.e. $\alpha_j = 0$ and $\Delta\alpha = 0$, the signal intensity dependence is given by the well known equation

$$I \sim |\chi^{(3)}|^2 I_p^2 I_s L^2 \operatorname{sinc}^2(\Delta\beta L/2) \quad (5)$$

In the phase-matched case (i.e. $\Delta\beta = 0$), the signal intensity increases with the square of the length, and in the phase-mismatched case (i.e. $\Delta\beta \neq 0$) it is seen that the signal intensity shows oscillations depending on the length, which results from interference effects due to the coherent nature of the signal. The period of oscillation is determined by twice the coherence length $L_{COH} = \pi/\Delta\beta$.

It can be shown that, whenever the total cuvette length ($L = 2L_G + L_S$) equals 2 L_{COH}, the non-resonant signals generated in the glass, solvent and glass layers destructively interfere to zero, while the vibration resonant signal built up in the sample layer does not vanish since $L_{SAMPLE} < 2L_{COH}$, yielding a background-free resonant signal (see Fig. 2).

The main task now is to keep twice the coherence length equal to the total cuvette length. This can be done experimentally by adjusting the crossing angle η between the pump and Stokes beams (i.e. phase mismatching).

In the case of absorbing media, and under resonant excitation conditions, absorption of the beams may affect the coherence length depending on the value of $\Delta\alpha$. In some cases a full destructive interference may not be reached, which lowers the background suppression efficiency, since only the real part of the (complex) background can be suppressed in this way. However, since the complex background arises from the dissolved molecules at low concentration while the solvent produces mainly a real background, a large background suppression is expected.

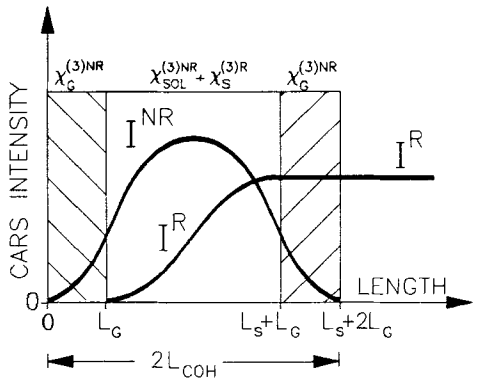

Figure 2. Schematic illustration of the non-resonant and resonant CARS intensities built up in the glass–sample–glass cuvette in the phase-mismatching configuration (after Ref. 19). The non-resonant signal arises from the glass layers [length L_G and non-resonant susceptibility $\chi_G^{(3)NR}$] and from the solvent in the sample layer L_s [non-resonant susceptibility $\chi_{SOL}^{(3)NR}$]. When the total cuvette length $2L_G + L_S$ equals $2L_{COH} = 2\pi/\Delta\beta$, with $\Delta\beta$ the phase-mismatch factor, the non-resonant CARS signal vanishes by destructive interference. The vibration resonant signal arising from dissolved molecules in the sample layer [resonant susceptibility $\chi_S^{(S)R}$] does not vanish since $L_s < 2L_{COH}$.

The important advantage of the PMM-CARS method is that this suppression technique is based on coherent cancellation and does not use the polarization character of the non-resonant and resonant signals. This means that the PMM-CARS and PCARS techniques can be combined to measure $\chi^{(3)R}$ components efficiently. Vibrations with polarization vectors $\mathbf{P}^R$ closely directed along the non-resonant polarization vector $\mathbf{P}^{NR}$ (or with ρ^R close to ρ^{NR}) are not suppressed when using PMM-CARS, in contrast to the case when PCARS is used. In the combination of PMM-CARS and PCARS the $\chi^{(3)R}_{1111}$ and $\chi^{(3)R}_{1221}$ components can be measured without interference of the non-resonant background, which in principle allows a straightforward estimation of depolarization ratios.

CARS fit procedure

The model used to fit the CARS spectra in the least-squares procedure is given by

$$F(x) = \chi(x)\chi(x)^* \quad (6)$$

where

$$\chi(x) = \left[f^{NR}\chi^{NR} + \sum_t f_t^R \frac{A_t^R \exp(i\theta_t^R)}{(\Omega_t - x)/\Gamma_t - i}\right] C \quad (7)$$

with f^{NR}, f_t^R and χ^{NR} = polarization factors defined in Eqns (A9), (A10) and (A7) in Appendix A, A_t^R = vibration resonant amplitude, θ_t^R = vibration resonant phase, Ω_t = vibration resonant frequency, x = a variable representing the frequency shift $\omega_p - \omega_s$, Γ_t = vibration resonant band width and C = scaling parameter.

The fit program enables us to fit simultaneously several spectra measured under different polarization conditions with a single set of parameters. Further, all parameters given in the fit function [Eqns (6) and (7)] can be used as free fit parameters. The problem to be solved is to find the minimum of

$$\sum_j \sum_i [I_j(x_i) - F_j(x_i)]^2 \tag{8}$$

where $I_j(x_i)$ are measured PCARS intensities at spectrum points x_i under polarization condition j and $F(x)$ is defined in Eqn (6). For the phase-mismatched spectra the non-resonant background was set to zero; $f^{NR} = 0$.

Raman and CARS excitation profiles

From Albrecht's vibronic theory of resonance Raman scattering, under the Born–Oppenheimer approximation (separation of the wavefunctions into electronic and vibrational parts) the Raman polarizability tensor α_{if} for the transition $i \to f$ can be written [21] as

$$\alpha_{if}(\omega) = A + B$$
$$= \frac{1}{\hbar} \sum_{k,v} \left[M_k{}^2 \langle f|v\rangle\langle v|i\rangle + \sum_{s \neq k} \frac{M_k h_{ks} M_s}{\hbar(\omega_k - \omega_s)} \times (\langle f|Q|v\rangle\langle v|i\rangle + \langle f|v\rangle\langle v|Q|i\rangle) \right] \times \frac{1}{\omega_{kv} - \omega_{gi} - \omega - i\Gamma} \tag{9}$$

where M_k denotes the electronic transition dipole moment, $\hbar\omega_{kv} = \hbar\omega_{k0} + \hbar\omega_v$ gives the energy of the state $|k\rangle|v\rangle$ and $\hbar\omega_{gi} = \hbar\omega_{g0} + \hbar\omega_i$ the energy of the state $|g\rangle|i\rangle$; ω denotes the frequency of the exciting laser beam, Γ the homogeneous line width of the resonant state, $\langle f|v\rangle$ the Franck–Condon overlap integrals, Q is the normal mode coordinate, v runs over vibrational states, whereas k and s run over electronic states, with frequencies ω_k and ω_s, and $h_{ks} = \langle s|\partial H/\partial Q|k\rangle$ is the vibronic coupling matrix element, with H the vibrational hamiltonian.

Usually the A term is largest for strongly allowed electronic transitions, thereby enhancing totally symmetric transitions. For example, this is the case when exciting in the Soret absorption band of D_{4h} symmetry porphyrins; the spectrum is dominated by totally symmetric (polarized) A_{1g} bands.[22]

The coupling element h_{ks} represents the mixing of states, through which weakly allowed vibrational transitions may gain intensity, in particular when the electronic states k and s are close in energy. This coupling has shown to be important in many porphyrin structures when exciting in the weaker electronic Q bands, where B_{1g}, B_{2g} (depolarized) and even A_{2g} (anomalously polarized) bands dominate the spectrum.[22]

The intensity dependence of Raman (and CARS) scattering on the excitation (pump) frequency (so-called Raman and CARS excitation profiles, REP and CEP, respectively) can be calculated using transform theory. This transform method relates the Raman intensity to the electronic absorption spectrum through a Kramers–Kronig (KK) relationship. For the fundamental transition $0 \to 1$, the REP can be written as[20,23–25]

$$\mathrm{REP}(\omega) \sim |\alpha_{01}(\omega)|^2 \sim S_1 |(1 + C_r)A(\omega) - (1 - C_r)A(\omega - \omega_1)|^2 \tag{10}$$

with $S_1 = \Delta^2/2$ a scaling parameter related to the dimensionless displacement Δ between harmonic oscillator potential curves representing electronic levels, C_r is a measure of vibronic coupling or non-Condon to Condon scattering [i.e. $C_r = (B + C)/A$, where A (Condon), B (Herzberg–Teller) and C (Jahn–Teller) are the terms that make up the scattering tensor in Albrechts theory]; ω_1 denotes the vibrational shift for which the REP is calculated. The function $A(\omega)$ is given by

$$A(\omega) = P \int_0^\infty \frac{\sigma_A(\omega')}{\omega'(\omega' - \omega)}\, d\omega' + i\pi \frac{\sigma_A(\omega)}{\omega} = Re\{A(\omega)\} + i\, Im\{A(\omega)\} \tag{11}$$

with $\sigma_A(\omega)$ the optical absorption cross-section at frequency ω, directly obtained from the measured absorption spectrum, and P denotes the principal of the integral. The function $A(\omega - \omega_1)$ in Eqn (10) is obtained from Eqn (11) with the shifted argument $\omega - \omega_1$. The real and imaginary parts of $A(\omega)$ are related to each other through the KK (or Hilbert) transform. In practice, the imaginary part is obtained directly from a digitized absorption spectrum, and the function $A(\omega)$ is computed by the method described in Ref. 25.

In the case of CARS the measured intensity is proportional to the absolute square of the third-order susceptibility tensor $\chi^{(3)}$. For totally symmetric modes and linear polarizations of the incident electric fields the amplitude $\chi^{(3)R}$ can be written as[26]

$$\chi^{(3)R}_{1111} = \frac{N}{3\hbar}(\bar{\alpha}^2 + \tfrac{4}{45}\bar{\gamma}_s{}^2) \tag{12}$$

$$\chi^{(3)R}_{1221} = \frac{N}{3\hbar}(-\tfrac{1}{9}\bar{\gamma}_a{}^2 + \tfrac{1}{15}\bar{\gamma}_s{}^2) \tag{13}$$

where N is the number of molecules and $\bar{\alpha}^2$, $\bar{\gamma}_s{}^2$ and $\bar{\gamma}_a{}^2$ are the CARS analogues of the isotropic, symmetric and anti-symmetric anisotropic Raman tensor invariants α^2, $\gamma_s{}^2$ and $\gamma_a{}^2$, given by[27] (with $i, j = x, y, z$)

$$\bar{\alpha}^2 = \frac{1}{9}\left[\sum_i (\alpha'_{ii})\right]\left[\sum_i (\alpha''_{ii})\right] \tag{14}$$

$$\bar{\gamma}_s{}^2 = \frac{1}{4}\sum_{\substack{i<j \\ i\neq j}} \left[2(\alpha'_{ii} - \alpha'_{jj})(\alpha''_{ii} - \alpha''_{jj}) + 3(\alpha'_{ij} + \alpha'_{ji})(\alpha''_{ij} + \alpha''_{ji}) \right] \tag{15}$$

$$\bar{\gamma}_a{}^2 = \frac{3}{4}\sum_{\substack{i<j \\ i\neq j}} (\alpha'_{ij} - \alpha'_{ji})(\alpha''_{ij} - \alpha''_{ji}) \tag{16}$$

where α' and α'' are given by

$$\alpha'_{\sigma\rho} = C \sum_k \left(\frac{M^\sigma_{gk} M^\rho_{kt}}{\omega_{kg} - \omega_a - i\Gamma_{kg}} + \frac{M^\rho_{gk} M^\sigma_{kt}}{\omega_{kg} + \omega_p + i\Gamma_{kg}} \right) \tag{17}$$

$$\alpha''_{\sigma\rho} = C \sum_k \left(\frac{M^\sigma_{tk} M^\rho_{kg}}{\omega_{kg} - \omega_p - i\Gamma_{kg}} + \frac{M^\rho_{tk} M^\sigma_{kg}}{\omega_{kg} + \omega_s - i\Gamma_{kg}} \right) \tag{18}$$

which correspond to the Raman pairs $\alpha'(\omega_p, \omega_a)$ and $\alpha''(\omega_p, \omega_s)$ that build up the vibration resonant susceptibility $\chi^{(3)}(\omega_a; \omega_p, \omega_p, -\omega_s) \sim \alpha(\omega_p, \omega_s)\alpha^*(\omega_p, \omega_a)$, and where σ, ρ denotes the applied polarizations (x, y or 1, 2), and M^{σ}_{gk} denotes the transition dipole moment.

Considering totally symmetric modes, (neglecting the anti-symmetric part), it follows from Eqns (12) and (13) that

$$\chi^{(3)R}_{1111} \sim (1 - \tfrac{4}{3}\rho^R)^{-1}\bar{\alpha}^2 \quad (19)$$

and for the CEP $\sim |\chi^{(3)R,t}_{1111}|^2$ a similar relationship to that given in Eqn (10) results:

$$\mathrm{CEP}(\omega) \sim |K(S_1)[(1 + C_a)A(\omega + \omega_1) - (1 - C_a)A(\omega)] \times [(1 + C_a)A(\omega) - (1 - C_a)A(\omega - \omega_1)]|^2 \quad (20)$$

where $K(S_1)$ is scaling parameter and C_a contains the vibronic coupling parameter C_r with $C_a = C_r S_1^{-1/2}$. It is seen from Eqn (20) that in CARS the CEP depends on $A(\omega)$, $A(\omega - \omega_1)$ and $A(\omega + \omega_1)$, corresponding to resonances at zero, Stokes and anti-Stokes shifts from the electronic transition, yielding more complicated excitation profiles compared to REPs. Equations (10) and (20) are used to calculated REPs and CEPs for pheophytin *b*.

EXPERIMENTAL

The Pheophytin *b* molecule

The molecular structure[4] of the pheophytin *b* (Pheo *b*) molecule is given in Fig. 3 in the inset. The calculated molecular weight M is 885.16 and its empirical formula is $C_{55}H_{72}O_6N_4$. The molecule consists of a tetrapyrrole ring, common in porphyrin structures, but with a fifth pyrrole ring attached to the pyrrole ring III. In chlorophyll *a* (Chl *a*) and chlorophyll *b* (Chl *b*), a magnesium atom is positioned at the centre of the molecule. The difference between the Chl *a* and Chl *b* molecules is the preserve of a methyl group (CH_3) in Chl *a* and an aldehyde group (COH) in Chl *b* at the C-3 position. In the pheophytins the central Mg atom is replaced by two H atoms. Pheo *b* appears in leaf extracts, and is assumed to be formed as a result of decomposition of Chl *b* during the extraction.

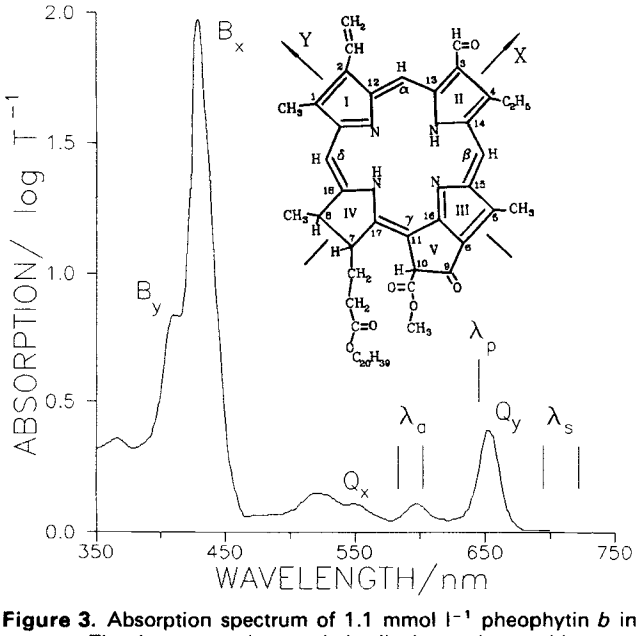

Figure 3. Absorption spectrum of 1.1 mmol l^{-1} pheophytin *b* in acetone. The degenerate (*x*, *y*-polarized) electronic transitions are denoted by $Q_{x,y}$ and $B_{x,y}$. Excitation conditions of the pump, Stokes and CARS signal wavelengths are indicated by the vertical lines. The molecular structure and molecular *x*, *y*-axes of Pheo *b* are given in the inset.

Sample preparation

Chl *b* extracted from spinach and substantially free from Chl *a* was purchased from Sigma (Lot No. 58F-9510) and used without further purification. A 5 mg amount of Chl *b* was dissolved in 5 ml of acetone (100%, GR grade, purchased from Merck). For the pheophytinization of the Chl *b*, 0.25 ml of 0.12 mol l^{-1} HCl was added, thereby removing the central magnesium atom and replacing it by two hydrogen atoms. With a molecular weight of 907.5 for Chl *b*, the concentration of the Pheo *b* was calculated to be 1.1×10^{-3} mol l^{-1}. Acetone was chosen as a solvent to be sure that only monomeric Pheo *b* was present. Further, the small number of Raman-active vibrations of the solvent (compared with, for instance, diethyl ether) allows an easy interpretation of the measured spectra. The absorption spectrum of Pheo *b* in acetone and the excitation conditions are given in Fig. 3.

As a result of the lowering of the D_{4h} symmetry of the porphyrin ring by the presence of the fifth ring, the absorption spectrum clearly shows the degenerate electronic Q and B transitions indicated by Q_y, Q_x, B_x and B_y and some vibronic progressions, (the molecular *x*- and *y*-axes are indicated in Fig. 3). From the amplitude ratio between the absorption of the B_x and Q_y bands we conclude that with this procedure a full conversion from Chl *b* to Pheo *b* is obtained.[4] No additional process was carried out to remove the magnesium chloride or the excess of hydrochloric acid from the sample. The sample was sealed and stored in the dark at 4 °C. During the experiments [at room temperature (22 °C)] the solution was flushed with dry nitrogen to deoxygenate the sample. Since the purge with nitrogen resulted in strong evaporation of the acetone, the sample container was constantly refilled with fresh pure acetone, thereby keeping the Pheo *b* concentration constant.

Experimental CARS set-up

The optical layout of the CARS spectrometer is shown in Fig. 4. The second harmonic of an Nd:YAG laser operated at 10 Hz with 8 ns pulse duration pumps two PDL2 dye lasers. The pump beam (ω_p) of the CARS process is provided by the first dye laser containing dichloromethane, which is tunable in the 620–660 nm range. The second dye laser containing LDS and tunable in the 680–725 nm range delivered the Stokes beam (ω_s) of the CARS process. The delay lines are adjusted to ensure that the pump and Stokes pulses temporally overlap at the sample position. The beam

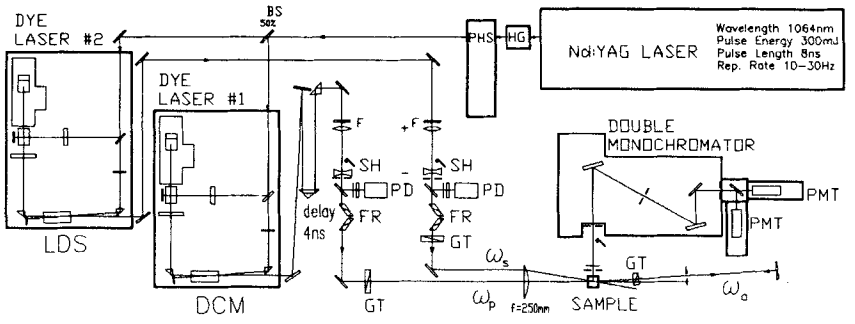

Figure 4. Optical layout of the CARS spectrometer. HG = harmonic generator; PHS = prism harmonic separator; BS = beamsplitter; F = filter; SH = shutter; PD = photodiode; FR = double Fresnel Rhomb; GT = Glan–Taylor polarizer; PMT = photomultiplier tube.

diameters are compressed by telescopes to about 1–2 mm. Parts of the beam are detected by PIN photodiodes for referencing and monitoring the intensities. Double Fresnel rhombs and high-quality Glan–Taylor polarizers are used to control and upgrade the linear polarizations of the beams. The beams are focused in the cuvette by a 250 mm lens. Focal diameters in the curvette are 150 μm. Pulse energies are 290 μJ for the pump beam and 400 μJ for the Stokes beam. The crossing angles of the pump and Stokes beams to obtain phase matching (or phase mismatching) can be adjusted by changing the distance of the parallel pump and Stokes beams on the lens via the mirror M on a stepper motor-driven translation stage. The CARS signal is analysed by a Glan–Taylor polarizer and collected by a spherical mirror on a rotatable mount with the axis of rotation coinciding with the vertical axis of the cuvette. The signal is deflected on to a mirror on this axis beneath the cuvette and focused on the entrance slit of a double monochromator (UV–visible, 200 mm, Jobin Yvon) and detected by a water-cooled photomultiplier-tube (RCA 9973B). The computer and electronics are interfaced by an IEEE bus. Signals are digitized in an eight-channel 12-bit ADC and stored on floppy disks for later analysis. Automatic selection of the dye lasers and monochromator wavelength, crossing angles and collection angles are achieved by computer control of the stepper motors. The crossing angle η between $\mathbf{k}_p$ and $\mathbf{k}_s$ and the collection angle v between $\mathbf{k}_p$ and $\mathbf{k}_a$ (see Fig. 5) are predetermined for different frequencies and stored in angle files used in the computer program controlling the spectral scan. The spectra were recorded with a spectral resolution of 2 cm^{-1} and each point was averaged over 50 laser shots. The spectra were corrected for intensity fluctuations and dye laser efficiency and smoothed using a five-point Savitsky–Golay smoothing procedure.[28]

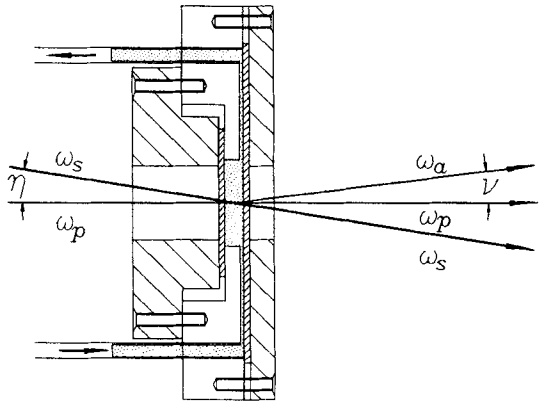

Figure 5. Layout of the flow cuvette. The small-hatched areas indicate glass window layers and the dotted area indicates the sample layer. Glass windows and sample layers are held together by two plates (large-hatched area), with central openings for the laser beams. The sample solution is circulated through the cell by a peristaltic pump. Pump and Stokes beam crossing angle and CARS signal collection angle are denoted by η and v, respectively.

In the CARS measurements the sample was flushed through a flow cuvette by means of a peristaltic pump. The layout of this cuvette is shown in Fig. 5. With a flow rate of 2 μl s^{-1} which results in a flow of 300 μm per pulse at the sample position, and a laser focus diameter of 150 μm, the volume probed by the CARS beams is refilled with new sample for each laser shot. The windows of the cuvette are 0.15 mm microscopic coverslides, anti-reflection coated on their air–glass interface to minimize multiple interference effects in the measured spectra.[14] The sample length used is 0.25 mm. Although this is smaller than the optimum sample length,[14] which is about 0.6 mm for an $N = 1.1$ mmol l^{-1} concentration Pheo *b* in acetone in the 1100–1700 cm^{-1} range, this length was chosen for reasons of applicability of the PMM-CARS technique which works well for the 0.15 mm–0.25 mm–0.15 mm glass–sample–glass configuration. A 0.6 mm sample length requires 0.3–0.4 mm (anti-reflection coated) glass windows, which were not available at the time of the experiment. Moreover, the cuvette configuration used, yielded signal levels high enough to perform the measurements.

RESULTS

Phase-matched resonance CARS spectra

Resonance (phase-matched) CARS spectra proportional to $|\chi^{(3)}_{1111}|^2$ and $|\chi^{(3)}_{1221}|^2$ of 1.1 mmol l^{-1} Pheo *b* in acetone solution in the 1100–1650 cm^{-1} range are shown in Fig. 6. The scale of the $|\chi^{(3)}_{1221}|^2$ spectrum is enlarged 9.96 times, which yields an estimated value for the non-resonant depolarization ratio of $\rho^{NR} = 0.317$, close to 1/3 as expected for a transparent isotropic medium (Kleinman symmetry). The differences in the two susceptibility components show deviations of the vibrational depolarization ratios from the non-resonant depolarization ratio. The background present in these spectra is the non-resonant background contribution mainly from the solvent. A direct depolarization estimation from these spectra is obstructed by the complex

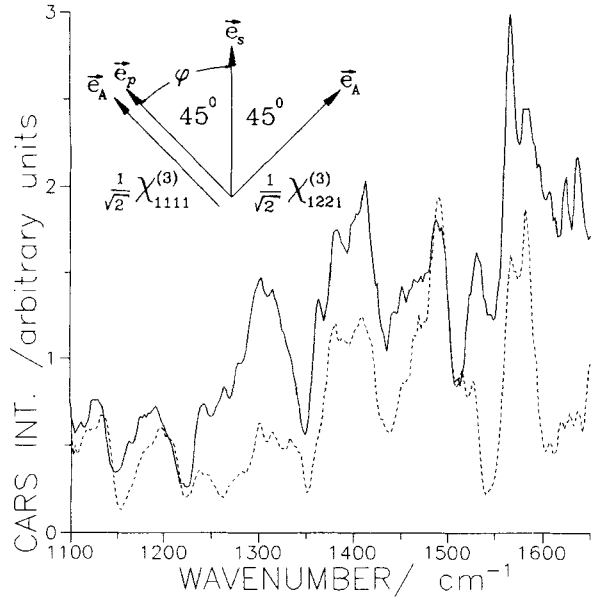

Figure 6. Phase-matched resonance $|\chi^{(3)}_{1111}|^2$ (solid line) and $|\chi^{(3)}_{1221}|^2$ (dashed line) CARS spectra of a 1.1 mmol l^{-1} Pheo *b* in acetone solution in the 1100–1650 cm^{-1} range. Polarization orientations of pump, Stokes and analyser are indicated. The scale of the $|\chi^{(3)}_{1221}|^2$ spectrum is enlarged by a factor of 9.96. This indicates that the non-resonant depolarization ratio $\rho^{NR} = 0.317$, close to 1/3 (Kleinman symmetry).

line shapes caused by the interference of the non-resonant background with vibration resonant signals. Assignment of band positions to the maxima, as is often done, does not seem reliable in this case.

Phase-matched resonance PCARS spectra

Phase-matched resonance PCARS spectra of 1.1 mmol l^{-1} Pheo *b* in acetone solution in the 1100–1650 cm^{-1} range, measured with a polarization angle $\varphi = 60°$, are shown in Fig. 7. The angle for optimum suppression of the non-resonant background $\rho^{NR} = 0.317$ is calculated to be $\psi_0 = 61.2°$. The spectra in Fig. 7 were recorded with analyser settings ε away from ψ_0. The line shape changes observed at different analyser settings around the position of background suppression show the different polarization character of the bands. However, vibrational bands with depolarization ratios ρ^R close to ρ^{NR} are suppressed together with the background. Estimation of depolarization ratios from these spectra is possible in principle, by curve fitting these spectra under different polarization conditions with a single set of band parameters.

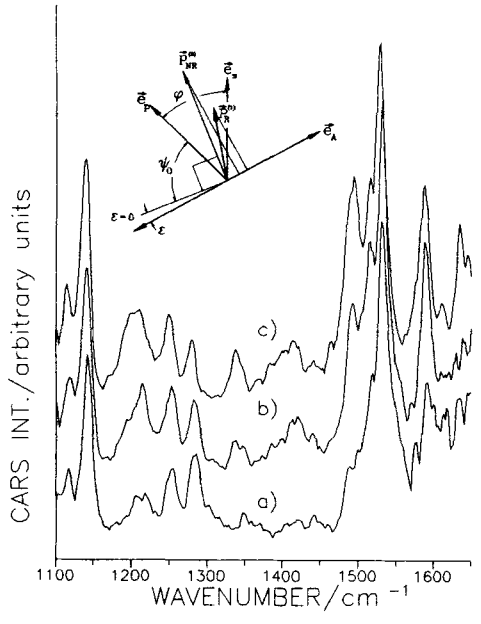

Figure 7. Phase-matched resonance PCARS spectra of 1.1 mmol l^{-1} Pheo *b* in acetone solution in the 1100–1650 cm^{-1} range. Polarization orientations of pump, Stokes and analyser are indicated, with $\varphi = 60°$. The analyser setting ε was varied around the angle $\psi_0 = 61.3°$ of background suppression: (a) $\varepsilon = +1°$; (b) $\varepsilon = 0°$; (c) $\varepsilon = -3°$.

Phase-mismatched resonance PCARS spectra

In Fig. 8 the phase-mismatched resonance PCARS spectra proportional to $|\chi^{(3)}_{1111}|^2$ and $|\chi^{(3)}_{1221}|^2$ of 1.1 mmol l^{-1} Pheo *b* in acetone solution in the 1100–1650 cm^{-1} range are presented. Polarization orientations of pump, Stokes and analyser are indicated, with $\varphi = 45°$. The scan was carried out with crossing angle (η) and collection angle (ν) adjustments according to $\eta(°) = 1.74 + 5.95 \times 10^{-4}\sigma$ and $\nu(°) = 1.88 + 2.90 \times 10^{-4}\sigma$, where σ is the shift in cm^{-1}. These angles are measured outside the sample (in air) relative to the pump beam direction (see also Fig. 5).

In these spectra the non-resonant background from acetone is suppressed by phase mismatching. The phase-mismatched spectra in Fig. 8 were recorded with a reduced collection iris diaphragm (0.8 mm at 200 mm from the sample, thus with a collection angle resolution of 0.22°) in the signal path. From the Lorentzian line shapes, band position assignments can be made more easily compared with the phase-matched spectra given in Fig. 6.

Dispersion of the CARS intensity

In Fig. 9, phase-mismatched $|\chi^{(3)}_{1111}|^2$ spectra of 1.1 mmol l^{-1} Pheo *b* in acetone solution are shown excited at different pump wavelengths in the 630–645 nm range. These spectra clearly indicate the dependence of the changes in band intensities on the excitation wavelength.

DISCUSSION

The clear difference between the phase-matched resonance CARS and PCARS spectra in Figs 6 and 7 shows the influence of the non-resonant background and polarization character of the many interfering Raman bands present in this spectral region. The more Lorentzian-like band shapes and improvement of resonant to (non-resonant) background ratio in the PCARS spectra of Fig. 7 is advantageous only for bands with depolarization ratios ρ^R different from $\rho^{NR} = 0.317$. The central part of the spectrum has almost vanished because the bands have ρ^R values which are close to ρ^{NR}. Comparing the phase-mismatched PCARS spectra of Fig. 8 with Figs 6 and 7, it is seen that the spectrum

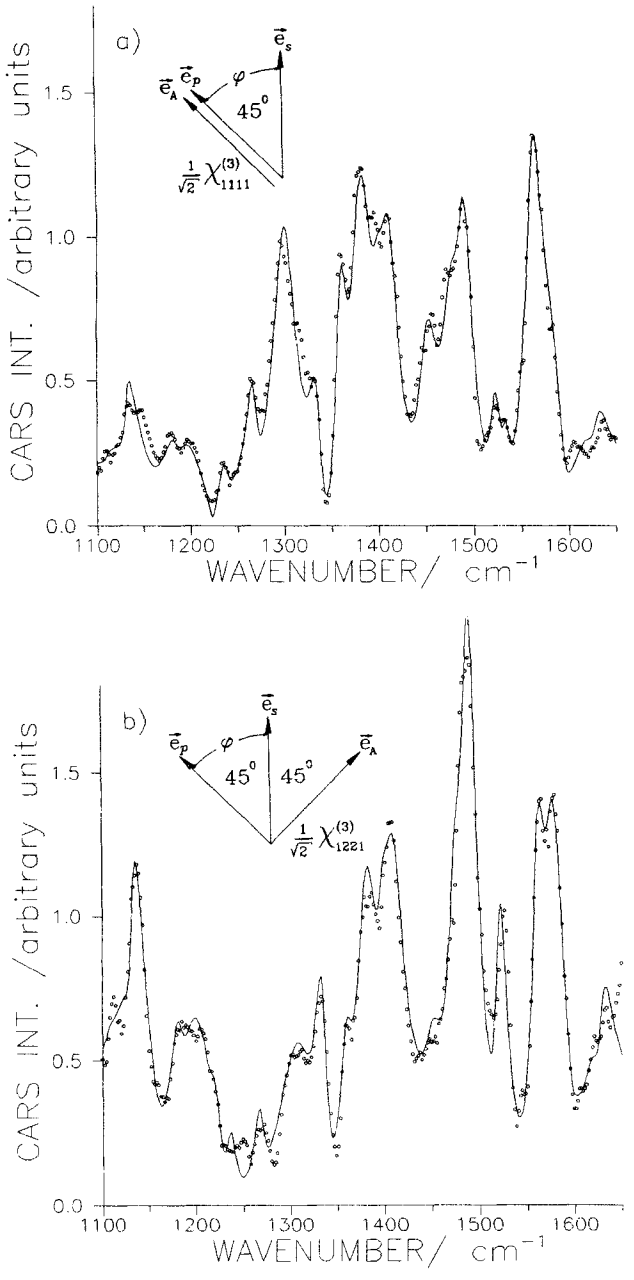

Figure 8. Phase-mismatched resonance PCARS spectra of 1.1 mmol l^{-1} Pheo *b* in acetone solution in the 1100–1650 cm^{-1} range, excited at pump wavelength $\lambda_p = 645$ nm: (a) $|\chi^{(3)}_{1111}|^2$; (b) $|\chi^{(3)}_{1221}|^2$. Points represent measured data and the solid lines are fitted results.

more resembles that of Fig. 6, but with improved resonant to background ratio, due to the phase mismatching. The $\chi^{(3)R}_{1111}$ and $\chi^{(3)R}_{1221}$ spectra in Fig. 8 clearly show their different polarization character. Around 1575 cm^{-1} a special feature is seen: the $\chi^{(3)R}_{1111}$ component shows a weak shoulder, whereas the $\chi^{(3)R}_{1221}$ component is large, which means that this band is anomalously polarized.

Although the non-resonant background from the solvent acetone is suppressed, the spectrum still contains interference between the resonant vibrations. The measured intensity in this case can be written as

$$I_{\text{PMM-CARS}} \sim \sum_r |\chi_r^{(3)R}|^2 + 2\sum_{r<s}\sum [Re\chi_r^{(3)R} Re\chi_s^{(3)R} + Im\chi_r^{(3)R} Im\chi_s^{(3)R}] \quad (21)$$

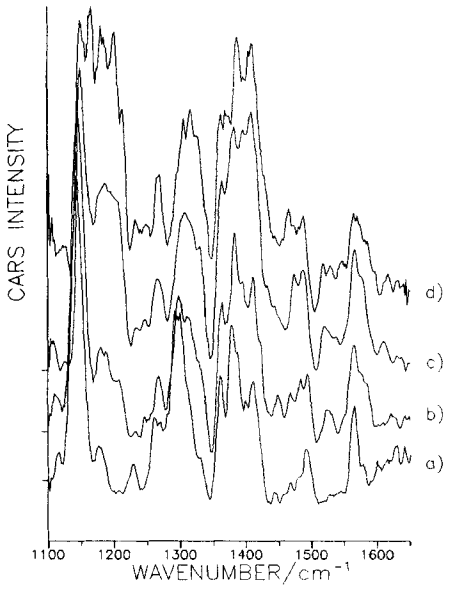

Figure 9. Phase-mismatched resonance PCARS spectra of 1.1 mmol l^{-1} Pheo *b* in acetone solution in the 1100–1650 cm^{-1} range, excited at different pump wavelengths: (a) $\lambda_p = 645$ nm; (b) $\lambda_p = 640$ nm; (c) $\lambda_p = 635$ nm; (d) $\lambda_p = 630$ nm. The spectra correspond to the $|\chi^{(3)}_{1111}|^2$ component and are drawn to the same vertical scale. Zero levels are indicated by the horizontal lines on the ordinate.

The first term gives Lorentzian Raman lines corresponding to a squared Raman spectrum and the second term contains cross-terms between the Raman bands.

In principle, the combined PMM-CARS and PCARS techniques yielding $\chi^{(3)R}_{1111}$ and $\chi^{(3)R}_{1221}$ components without an interfering non-resonant background could give a direct estimation of their (depolarization) ratios. However, in this case, the spectral range contains more than 30 bands and interference as shown in Eqn (21) makes this hardly possible.

Fitting programs are essential to estimate all band parameters. From the simultaneous fit on the two PMM-PCARS spectra, frequencies, band widths, amplitudes and depolarization ratios were obtained, which are listed in Table 1. A total of 31 bands (28 of Pheo *b* and 3 of acetone) were found. The phases of the solvent (acetone) bands were set to zero; the Pheo *b* vibrational phases were determined relative to the solvent phases. Although the non-resonant background is absent, vibrational phase differences still manifest themselves through band-to-band interference [see also Eqn (21)].

The band assignments given in Table 1 were taken from Ref. 29. Most frequencies found for Pheo *b* are in good agreement with Raman and CARS data for Pheo *b* and Chl *b*. Table 2 presents such a comparison. Discrepancies are found for the 1335, 1411, 1475, 1521, 1575 and 1601 cm^{-1} bands with more than five wavenumbers difference or which do not appear in the second or third column of Table 2. Different excitation conditions and samples may explain these differences. Another explanation would be the possibility of excited state bands, since the fluorescence lifetime of Pheo *b* in acetone is a few nanoseconds,[30] which is comparable to our pulse duration and may lead to build-up of excited singlet S_1 state population and triplet T_1 population after intersystem crossing from the S_1 state. Some of these band frequencies (1335, 1475 and 1575 cm^{-1}) are close to triplet T_1 state band frequencies observed for

Table 1. Pheo *b* band parameters estimated from a simultaneous non-linear least-squares fit on the $\chi^{(3)R}_{1111}$ and $\chi^{(3R}_{1221}$ (phase-mismatched) spectra of Fig. 8

Ω_t (cm^{-1})	Γ_t cm^{-1}	A_t^R (a.u.)	θ_t^R (°)	ρ_t^R	Assignments[29]
1110	3.0	0.03	180	0.00	
1132	5.2	0.26	−117	0.43	
1145	20.2	0.37	60	0.80	
1151	20.4	0.21	0	0.70	
1182	8.0	0.13	24	0.36	$\nu C_m C_{10}$(IV), $\gamma C_b H$(IV)
1205	25.0	0.61	23	0.57	$\gamma C_b H$(IV), $\gamma C_m H(\delta)$
1220	6.4	0.11	0	0.70	Acetone
1224	5.9	0.31	176	0.00	$\delta C_b H$(IV), $\nu C_a N$(IV), $\delta C_m H(\alpha)$
1236	6.0	0.21	−20	0.50	$\delta C_b H$(IV), δCH(V−10)
1268	6.0	0.38	9	0.30	$\delta C_m H(\alpha, \beta)$
1301	11.4	0.56	−16	0.00	$\nu C_a N$(II), $\nu C_a N$(IV)
1314	25.0	0.81	37	0.37	$\nu C_a N$(II), $\nu C_a N$(IV)
1335	8.5	0.74	26	0.39	δCH_2(scissors)
1355	17.2	0.28	0	0.78	Acetone
1360	7.5	0.73	−29	0.14	$\nu C_a N$
1380	16.4	1.29	−27	0.31	$\nu C_a N$(IV), $\nu C_a N$(I, III)
1397	7.0	0.17	−63	0.53	$\nu C_a C_b$(II), $\nu C_a C_m(\alpha, \delta)$
1411	10.8	0.58			
1428	40.0	0.22	0	0.70	Acetone
1450	12.8	0.62	−10	0.16	γCH_2(V) scissors, $\nu C_a C_m(\gamma, \delta)$
1475	12.0	0.61	4	0.42	
1489	9.0	0.70	9	0.50	$\nu C_a C_b$(I), $\nu C_a C_m(\delta)$
1521	7.2	0.47	15	0.55	$\nu C_a C_b$(I), $\nu C_a C_b$(III)
1532	4.3	0.20	0	0.05	$\nu C_b C_b$(I), $\nu C_a C_b$(III)
1551	15.1	0.63	−5	0.23	
1561	8.7	0.74	1	0.35	$\nu C_a C_b$(III), $\nu C_b C_b$(I)
1575	10.0	0.09	−4	2.10	$\nu C_b C_b$(I), $\nu C_a C_b$(III)
1593	10.4	0.45	−163	0.29	$\nu C_a C_m(\alpha, \beta)$
1601	24.2	0.26	0	0.30	$\nu C_a C_m(\alpha, \beta)$
1615	8.0	0.07	0	0.71	$\nu C_a C_m(\alpha, \beta)$
1629	8.0	0.20	0	0.58	$\nu C_a C_m(\gamma)$

example in bacteriochlorophyll.[30] Intersystem crossing from the excited singlet S_1 state to the triplet T_1 state usually is high[30] (>50%) in these molecules; however, the conditions for the CARS process in the T_1 state are off-resonance since the nearest $T_n \leftarrow T_1$ absorption probably lies in the 420 nm range[30,31] and we therefore expect a low contribution from this state.

From the estimated depolarization ratios in Table 1, it follows that the 1575 cm^{-1} band is anomalously polarized ($\rho^R > 1$). This is surprising since most Raman data have revealed mainly polarized bands. The depolarization ratios of the other bands are in reasonable agreement with the data avaiable from PCARS on Chl *b*,[14] but the latter spectra were fitted manually and fewer bands were used in the same spectral range.

Resonance Raman and CARS scattering symmetries are determined by the symmetry of the molecule. For metalloporphyrins, with the most pronounced electronic transitions in the plane of the molecule, the D_{4h} symmetry leads to in-plane Raman modes of A_{1g} (polarized), A_{2g} (anomalously polarized) and B_{1g}, B_{2g} (depolarized) symmetry. The non-totally symmetric vibrations, for example of A_{2g} symmetry, gain their intensity by vibronic coupling with nearby electronic states. The symmetry of the Pheo *b* molecule is lost by the presence of the fifth pyrole ring, which lowers the D_{4h} symmetry actually to C_1. However, in this case only totally symmetric (polarized) bands described by Albrecht's *A* term are expected. That this is not the case is clear from the fit and depolarization ratios, which vary from polarized, depolarized, and anomalously polarized. This also shows that non-Condon (*B* + *C* terms) scattering mechanisms are active in this excitation region. From these facts it follows that the Pheo *b* molecule probably has an effective symmetry between C_1 and D_{4h} (such as C_{2v}). From a comparison of resonance Raman spectra and normal-mode calculations of model Ni–metalloporphyrins with lowered symmetry D_{4h}, C_{2v} and C_1, Boldt *et al.*[29] concluded that, under excitation in the Q_y band, B_{2g} (depolarized) modes are enhanced and that vibronic coupling from the *Q* and *B* or Soret states is present in these molecules. It is highly likely that the same applies to the Pheo *b* molecule. The presence of the anomalously polarized 1575 cm^{-1} band may be caused by vibronic coupling of the Q_y band with the B_y (Herzeberg–Teller *B* term) or even with the Q_x band (intra-Jahn–Teller) (but not from ground state–excited state coupling Jahn–Teller or *C* term).

REPs of Ni–Pheo *a* excited in the Q_y region measured by Mattioli *et al.*[8] indicate that vibronic coupling mechanisms are responsible for up to 40% [parameter $C_r = 0.4$ in Eqn. (10)], which explains the asymmetric enhancement of modes in the Q_{0-1} region. The simulated REP calculations on Ni–Pheo *a* indeed showed symmetric enhancement of modes in the Q_{0-0} band for $C_r = 0$ (no vibronic coupling) and asymmetric enhancement with maxima around the shifted vibrational frequency from the 0–0 frequency with C_r ranging from 0

Table 2. Comparison of estimated Pheo *b* Raman shifts (in cm^{-1}) with data from spontaneous Raman (Refs 5 and 6), and resonance CARS (Refs 11 and 14) and Raman shifts of Chl *b*[a]

Pheophytin *b*			Chlorophyll *b*		
PMM-CARS[b] (λ_e = 645 nm)	RS[6] (λ_e = 459 nm)	RS[5 c] (λ_e = 459 nm)	CARS[11] (λ_e = 694.3 nm)	RS[6] (λ_e = 459 nm)	PCARS[14] (λ_e = 645 nm)
1132 vw		1127 wsh		1128 m	
1145 m	1148 s	1150 s			
	1170 vwsh			1160 m	
1182 wm	1180 vwsh	1178 vw	1174 w	1177 ms	1174 m
			1191 vs	1190 ms	
1205 m	1205 sh	1205 sh	1214 m	1210 w	
1224 wm	1222 m	1225 m		1228 m	1225 m
			1256 vs		
1268 wm	1270 w	1271 w	1276 wm	1270 m	
					1286 w
1301 m		1302 wsh	1299 w	1295 m	
1314 ms	1308 w	1312 s	1310 wm	1309 vwsh	
1335 m		1341 s		1332 sh	1331 w
	1348 s		1344 s	1350 s	
1360 s	1358 vwsh	1355 s		1357 sh	
		1363 s(S)			1365 ms
1380 s	1375 sh	1380 sh		1380 sh	
			1387 m		1390 w
1397 m	1397 w	1399 m		1394 m	
1411 ms		1413 m	1417 m	1420 sh	
	1435 vwsh			1437 s	
1450 m	1443 w	1445 m	1458 w		
				1465 vw	1457 s
1475 s		1470 vw			
				1480 w	
1489 m	1485 vw	1490 m	1495 vs		1494 mw
1521 m				1523 wm	1525 w
1532 w	1534 s	1532 wsh	1528 w		
1551 m	1555 sh	1551 s			1551 vw
1561 s		1565 s	1563	1567 vs	
1575 w			1579 m		
1593 w	1587 wsh	1592 w			1590 vs
	1615 vw		1606 vw	1610 vw	1620 m

[a] vs = Very strong; s = strong; m = medium; ms = medium strong; w = weak; vw = very weak; wsh = weak shoulder.
[b] Fitted results.
[c] RS[5] solid deposit at 30 K.

to -0.9. In these calculations the shift parameter S_1 was set to 1, since we have no absolute values of REPs, and S_1 merely serves as a scaling parameter.

For the CEP calculations the shift parameter S_1 was obtained from a fit on the measured absorption spectrum. The model is based on the optical theorem which relates the optical absorption cross-section to the scattering tensor:[23]

$$\sigma_A(\omega) \sim \omega \text{ Im } \alpha(\omega) \tag{22}$$

where the latter involves Albrecht A and B terms (including vibronic coupling). Electronic transitions are modelled by the normal coordinate displaced harmonic oscillators similar to that in Eqn (10):

$$\sigma_A(\omega) \sim \omega \text{ Im } \alpha(\omega) \sim K \sum_{k,v} \left[M_k{}^2 |\langle v|0\rangle|^2 + \sum_{s \neq k} \frac{M_k h_{ks} M_s}{\hbar(\omega_k - \omega_s)} (\langle f|Q|v\rangle\langle v|0\rangle + \langle f|v\rangle\langle v|Q|0\rangle) \right] \times \frac{\omega\Gamma}{(\omega + \omega_v)^2 + \Gamma^2} \tag{23}$$

where K is a scaling parameter.

With this simple model, the Pheo *b* absorption spectrum could be fitted by using only a single vibrational progression per electronic transition to acount for the asymmetry and reproduce intermediate absorption features in Fig. 3. From this fit we obtained displacement values Δ of about 1, which were used in the CEP calculations.

In Fig. 10, the amplitude dispersion for several vibrations is given for a pump wavelength range of 630–645 nm, obtained from a fit on the spectra given in Fig. 9. The results presented in Fig. 10(a) are in agreement with calculated CEPs by applying transform theory for totally symmetric modes and neglecting depolarization dispersion, presented in Fig. 11. In varying the coupling parameter C_r up to ± 1, the CEPs do not change significantly in the measured range. Although only a short range was measured, the results in Fig. 10(b), which shows opposite behaviour, cannot be simulated with CEPs of totally symmetric vibrations by varying the vibronic coupling parameter. This means that the bands shown in Fig. 10(b) must have either non-totally symmetric character or significant depolarization dispersion. The former coincides with estimated

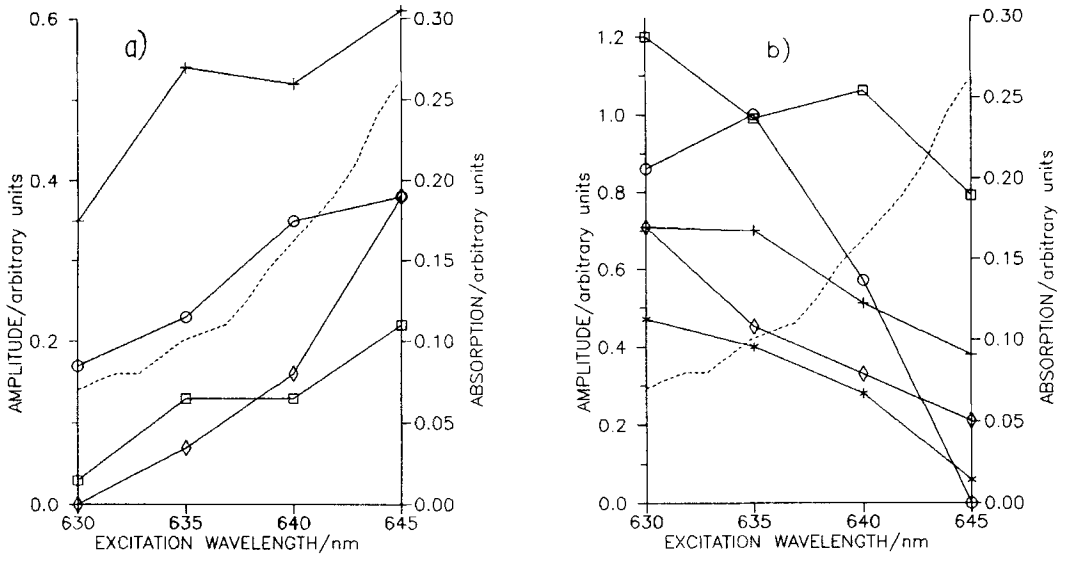

Figure 10. Raman band amplitude dispersion as estimated from fits on Fig. 9: (a), (◇) 1236, (○) 1450, (+) 1561 and (□) 1593 cm^{-1}; (b), (○) 1182, (□) 1314, (◇) 1397, (+) 1521 and (*) 1575 cm^{-1}. The dashed lines represent the absorption spectra in this interval.

depolarization ratios for the 1521 ($\rho^R = 0.68$) and 1575 cm^{-1} ($\rho^R = 2.25$) bands; however, the other bands are polarized, indicating that they have symmetrical character, which may indicate that depolarization dispersion may be neglected.

The mathematical procedure to calculate CEPs for non-totally symmetric modes (including the antisymmetric tensor $\gamma_a{}^2$) using transform theory is not yet available. Extension of the CEP model in this direction is necessary to understand fully the results obtained. Such an extension is not straightforward since for non-totally symmetric modes off-diagonal polarizability components α_{xy}, α_{yx}, etc., are involved, as can be seen from Eqns (12)–(16), which have no direct relationship to the absorption spectrum. An alternative approach could be to use linear or circular dichroism spectra for this purpose, although this complicates the technique further. Probable one must use the full expressions in Eqns (17) and (18), which again requires the sum-over-states approach. In addition, measurements of both amplitude and depolarization ratio dispersion over a wide spectral range are necessary to check theory.

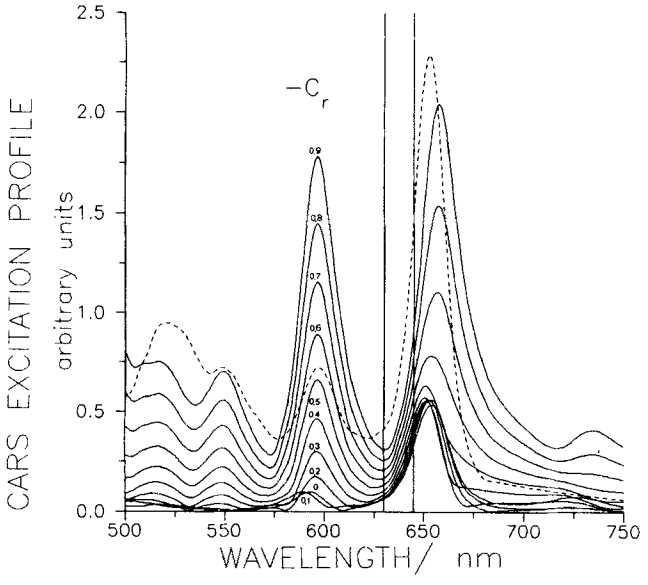

Figure 11. Calculated CARS excitation profile (CEP) for the totally symmetric mode at 1593 cm^{-1}, with $S_1 = 0.5$ and varying vibronic coupling parameter $C_r = 0$ to -0.9. The dashed line represents the absorption spectrum of Pheo *b*. The vertical lines indicate the measured spectral region.

CONCLUSION

We have demonstrated the unique possibilities of the combined phase-mismatched and polarization CARS technique on the highly fluorescing molecule Pheo *b* under resonance excitation conditions in the Q_y band to measure the $\chi^{(3)R}_{1111}$ and $\chi^{(3)R}_{1221}$ component spectra without background interference. From fits of these spectra we obtained a set of band parameters including depolarization ratios. The frequencies correspond well with data obtained by others, although some differences exist which may be caused by the use of different samples or excitation conditions, or attributed to the special resonance conditions of the more complex CARS process compared with the Raman process. Estimated depolarization ratios indicate that polarized and depolarized bands and one anomalously polarized band are present in the measured range. On the basis of C_1 symmetry of the Pheo *b* molecule one would expect polarized bands only, indicating that either the effective symmetry is not fully lost or that vibronic coupling mechanisms in the molecule enhance non-totally symmetric modes in this excitation region. The amplitude dispersion measurements can only partly be understood from CEP calculations of totally symmetric modes. The different dispersion behaviour of some bands point to their non-totally symmetric character, although some of these bands are polarized. These effects may be interpreted further if CARS excitation profile model calcu-

lations through transform methods are extended to include non-totally symmetric modes.

We think that the CARS measurements of the type shown can provide helpful additional information, in particular on the highly fluorescing chlorophyll and pheophytin molecules excited in the lowest electronic states, which are hardly accessible to RS. PMM-CARS measurements of amplitude and also depolarization dispersion of pheophytin molecules in the lowest electronic bands and theoretical extension of the CEP model are the subject of further research.

Acknowledgements

The authors thank Dr R. P. H. Kooyman and Professor Dr R. van Grondelle for valuable discussions.

REFERENCES

1. L. P. Vernon and G. R. Seeley, *The Chlorophylls*. Academic Press, New York (1966).
2. G. S. Marks, *Heme and Chlorophyll*, Van Nostrand, London (1969).
3. R. P. H. Kooyman, PhD Thesis, Agricultural University, Wageningen (1980).
4. L. P. Vernon, *Anal. Chem.* **32**, 1144 (1960).
5. M. Lutz, in *Advances in Infrared and Raman Spectroscopy*, edited by R. J. H. Clark and R. E. Hester, Vol. 11, p. 211. Heyden, London (1984).
6. M. Lutz, *J. Raman Spectrosc.* **2**, 497 (1974).
7. M. Lutz, *Biochim. Biophys. Acta* **460**, 408 (1977).
8. T. A. Mattioli, L. V. Haley and J. A. Koningstein, *Chem. Phys.* **140**, 317 (1990).
9. A. Lau, W. Werncke, J. Klein and M. Pfeiffer, *Opt. Commun.* **21**, 399 (1977).
10. E. Höxtermann, W. Werncke, I. N. Stadnichuk, A. Lau and P. Hoffmann, *Stud. Biophys.* **92**, 147 (1982).
11. E. Höxtermann, W. Werncke, J. T. Tschö, E. Brecht, A. Lau and P. Hoffmann, *Stud. Biophys.* **113**, 165 (1986).
12. E. Höxtermann, W. Werncke, J. T. Tschö, A. Lau and P. Hoffmann, *Stud. Biophys.* **115**, 85 (1986).
13. M. A. Yuratich and D. C. Hanna, *Mol. Phys.* **33**, 671 (1977).
14. T. A. H. M. Scholten, PhD Thesis, University of Twente (1989).
15. T. A. H. M. Scholten, G. W. Lucassen, F. F. M. de Mul and J. Greve, *Appl. Opt.* **27**, 3225 (1988).
16. T. A. H. M. Scholten, G. W. Lucassen, F. F. M. de Mul and J. Greve, *J. Raman Spectrosc.* **20**, 503 (1989).
17. G. W. Lucassen, T. A. H. M. Scholten, W. P. de Boeij, F. F. M. de Mul and J. Greve, in *Laser Applications in Life Sciences*, edited by S. A. Akhmanov and M. Yu. Poroshina, *Proc. SPIE* 1403, P. 185. (1991).
18. R. Brakel, V. Mudogo, and F. W. Schneider, *J. Chem. Phys.* **84**, 2451 (1986).
19. T. A. H. M. Scholten, G. W. Lucassen, F. F. M. de Mul and J. Greve, *Appl. Opt.* **28**, 1387 (1989).
20. P. M. Champion and A. C. Albrecht, *Chem. Phys. Lett.* **82**, 410 (1981).
21. A. C. Albrecht, *J. Chem. Phys.* **44**, 1476 (1961).
22. T. G. Spiro and X.-Y. Li, in *Biological Applications of Raman Spectroscopy*, edited by T. G. Spiro, Vol. 3, Chapt. 1. Wiley, New York (1988).
23. S. Hassing and O. Sonnich Mortensen, *J. Chem. Phys.* **73**, 1078 (1980).
24. B. R. Stallard, P. M. Champion, P. R. Callis and A. C. Albrecht, *J. Chem. Phys.* **78**, 712 (1983).
25. A. B. Myers and R. A. Mathies, in *Biological Applications of Raman Spectroscopy*, edited by T. G. Spiro, Vol. 2, Chapt. 1. Wiley-Interscience, New York (1987).
26. N. Watanabe, M. Shimizu and J. Tanaka, *J. Raman Spectrosc.* **18**, 381 (1987).
27. R. Igarashi, Y. Adachi and S. Maeda, *J. Chem. Phys.* **72**, 4308 (1980).
28. A. Savitzky and M. J. E. Golay, *Anal. Chem.* **36**, 1627 (1964).
29. N. J. Boldt, R. J. Donohoe, R. R. Birge and D. F. Bocian, *J. Am. Chem. Soc.* **109**, 2284 (1987).
30. E. Nishizawa, H. Hashimoto and Y. Koyama, *Chem. Phys. Lett.* **181**, 387 (1991).
31. J. F. Shepanski and R. W. Anderson, *Chem. Phys. Lett.* **78**, 165 (1981).

APPENDIX A. POLARIZATION CARS THEORY

The component i of the PCARS polarization vector is given by

$$P_i^{(3)} = \mathbf{e}_i \cdot \chi_{ijkl}^{(3)} \mathbf{e}_j \mathbf{e}_k \mathbf{e}_l^* E_j E_k E_l^*$$

where $i, j, k, l = x, y$ or 1, 2 (A1)

In Eqn. (A1) summation over repeated indices is assumed. The asterisks indicates that the photon is emitted. For an isotropic medium only three components $\chi_{ijkl}^{(3)}$ are independent, and the relationship between them is expressed by

$$\chi_{1111}^{(3)} = \chi_{1122}^{(3)} + \chi_{1212}^{(3)} + \chi_{1221}^{(3)} \quad \text{(A2)}$$

In single degenerate PCARS we have only two independent input polarization vectors, $\mathbf{e}_1 = \mathbf{e}_p$ and $\mathbf{e}_2 = \mathbf{e}_s$, and therefore $\chi_{1122}^{(3)}$ and $\chi_{1212}^{(3)}$ are indistinguishable. The projection of the CARS polarization vector on the analyzer unit vector is

$$\mathbf{e}_A^* \cdot \mathbf{P}^{(3)} = \mathbf{e}_A^* \cdot [(\chi_{1122}^{(3)} + \chi_{1212}^{(3)})\mathbf{e}_1(\mathbf{e}_1 \cdot \mathbf{e}_2^*) + \chi_{1221}^{(3)}\mathbf{e}_2^*(\mathbf{e}_1 \cdot \mathbf{e}_1)]E_1^2 E_2^* \quad \text{(A3)}$$

Defining the depolarization ratio by

$$\rho = \chi_{1221}^{(3)}/\chi_{1111}^{(3)} \quad \text{(A4)}$$

Eqn (A3) can be rewritten using Eqns (A2) and (A4):

$$\mathbf{e}_A^* \cdot \mathbf{P}^{(3)} = \chi_{1111}^{(3)}[(1-\rho)(\mathbf{e}_A^* \cdot \mathbf{e}_1)(\mathbf{e}_1 \cdot \mathbf{e}_2^*) + \rho(\mathbf{e}_A^* \cdot \mathbf{e}_2^*)]E_1^2 E_2^* \quad \text{(A5)}$$

It follows for the total contribution of non-resonant and resonant susceptibilities to the CARS intensity I_A

$$I_A \sim |(\mathbf{e}_A^* \cdot [\chi^{(3)NR} + \chi^{(3)R}]\mathbf{E}_1^2 \mathbf{E}_2^*)|^2 = \left| f^{NR}\chi^{NR} + \sum_t f_t^R \frac{A_t^R \exp(i\theta_t^R)}{-i + \Delta_t} \right|^2 \times I_1^2 I_2 M(\Delta k, L) \quad \text{(A6)}$$

where

$$\chi^{NR} = \chi_{1111}^{(3)NR} \quad \text{(A7)}$$

$$\frac{A_t^R \exp(i\theta_t^R)}{-i + \Delta_t} = \chi_{1111}^{(3)R,t} \quad \text{(A8)}$$

$$f^{NR} = (1 - \rho^{NR})(\mathbf{e}_A^* \cdot \mathbf{e}_1)(\mathbf{e}_1 \cdot \mathbf{e}_2^*) + \rho^{NR}(\mathbf{e}_A^* \cdot \mathbf{e}_2^*) \quad (A9)$$

$$f_t^R = (1 - \rho_t^R)(\mathbf{e}_A^* \cdot \mathbf{e}_1)(\mathbf{e}_1 \cdot \mathbf{e}_2^*) + \rho_t^R(\mathbf{e}_A^* \cdot \mathbf{e}_2^*) \quad (A10)$$

$$\rho^{NR} = \chi^{(3)NR}_{1221}/\chi^{(3)NR}_{1111} = \text{non-resonant depolarization ratio} \quad (A11)$$

$$\rho_t^R = \chi^{(3)R,t}_{1221}/\chi^{(3)R,t}_{1111} = \text{vibration resonant depolarization ratio} \quad (A12)$$

$$M(\Delta k, L) = e^{-(\Delta\alpha + \alpha_a)L}\left(\frac{\sinh(\Delta\alpha L/2) + \sin(\Delta\beta L/2)}{(\Delta\alpha L/2)^2 + (\Delta\beta L/2)^2}\right)L^2 = \text{phase match factor} \quad (A13)$$

where $\Delta\alpha = (2\alpha_p + \alpha_s - \alpha_a)/2$ with $\alpha_j = 2k_j''$ the exponential absorption coefficient and

$$\Delta\beta = n_a(\omega_a)\omega_a/c - |2k_p' - k_s'| = n_a(\omega_a)\omega_a/c - (4k_p'^2 + k_s'^2 - 4\cos\eta k_p' k_s')^{1/2}$$

with $\beta_j = k_j' = n_j(\omega_j)/c$ the real part of the wave vector, $n_j(\omega_j)$ the refractive index at frequency ω_j (j = p, s and a) and c the velocity of light in vacuum, and η the crossing angle of the pump and Stokes beam in the sample. Assuming linear polarization vectors and defining the axes as depicted in Fig. 1, the polarization factors f^N and f_t^R can be calculated as a function on the angles φ (between $\mathbf{e}_1$ and $\mathbf{e}_2$) and ψ (between $\mathbf{e}_1$ and $\mathbf{e}_A$):

$$f^{NR} = (1 - \rho^{NR})\cos\varphi\cos(\varphi + \psi) + \rho^{NR}\cos\psi \quad (A14)$$

$$f_t^R = (1 - \rho_t^R)\cos\varphi\cos(\varphi + \psi) + \rho_t^R\cos\psi \quad (A15)$$

Defining the angle between the polarization $\mathbf{e}_1$ and $\mathbf{P}^{NR,R}$ by $\theta^{NR,R}$, we can write

$$\tan\theta^{NR,R} = \mathbf{P}_y^{NR,R}/\mathbf{P}_x^{NR,R} \quad (A16)$$

It follows from Eqns (A3)–(A5) that

$$\theta^{NR,R} = \arctan(\rho^{NR,R}\tan\varphi) \quad (A17)$$

Full suppression of the non-resonant polarization is achieved at angles ψ_0 where $f^N = 0$ holds:

$$\psi_0 = \arctan(3/\tan\varphi) \quad (A18)$$

where Kleinmann symmetry is assumed:

$$\chi^{(3)NR}_{1111}/3 = \chi^{(3)NR}_{1122} = \chi^{(3)NR}_{1212} = \chi^{(3)NR}_{1221},$$

thus $\rho^{NR} = 1/3$.

APPENDIX B. PHASE-MISMATCHING CARS THEORY

The total CARS signal field E_{CARS} generated in the glass–sample–glass layer configuration can be written as[16]

$$E_{CARS} \sim e^{-1/2\alpha_c L_S}(E_G + E_S) \quad (B1)$$

where α_c is the absorption coefficient at the CARS frequency in the sample layer and E_G and E_S are the signal fields arising from the glass windows (length L_G) and sample layer (length L_S), respectively, which are given by

$$E_G = \mathbf{e}_c^* \cdot \chi_G L_G \times \text{sinc}(\phi_G)[\exp(i2(\phi_G + \phi_S) - \Delta\alpha L_S) + 1] \times \mathbf{e}_p\mathbf{e}_p\mathbf{e}_s^* \quad (B2)$$

$$E_S = \mathbf{e}_c^* \cdot \chi_S L_S \times \exp(i\phi_G)\left[\frac{\exp(i2\phi_S - \Delta\alpha L_S) - 1}{i2\phi_S - \Delta\alpha L_S}\right] \times \mathbf{e}_p\mathbf{e}_p\mathbf{e}_s^* \quad (B3)$$

with

$\mathbf{e}_c, \mathbf{e}_p, \mathbf{e}_s$ = unit polarization vectors of CARS signal, pump and Stokes beams;

$\chi_G = \chi^{(3)NR}_{GLASS}$ = non-resonant susceptibility of the glass window;

$\chi_S = \chi_S' + i\chi_S'' = \chi^{(3)NR}_{SAMPLE} + \chi^{(3)R,}_{SAMPLE} + i\chi^{(3)R,}_{SAMPLE}$ = non-resonant and resonant susceptibility of the sample layer;

$\Delta\alpha = (2\alpha_p + \alpha_s - \alpha_c)/2$ = absorption factor;

$\Delta\beta_G = (2k_p - k_s - k_c)_G$ = wave vector phase mismatch in the glass layers;

$\Delta\beta_S = (2k_p - k_s - k_c)_S$ = wave vector phase-mismatch in the sample layer;

$\phi_G = \Delta\beta_G L_G/2$ phase-mismatch factor in the glass layers;

$\phi_S = \Delta\beta_S L_S/2$ phase-mismatch factor in the sample layer.

Assuming that the polarization orientation of the non-resonant contributions of glass and sample layers are the same (transparent media which obey Kleinman symmetry), the non-resonant susceptibility of the sample layer χ_S^{NR} can be written as

$$\mathbf{e}_c^* \cdot \chi_S^{NR}\mathbf{e}_p\mathbf{e}_p\mathbf{e}_s^* = F\mathbf{e}_c^* \cdot \chi_G^{NR}\mathbf{e}_p\mathbf{e}_p\mathbf{e}_s^* \quad (B4)$$

where $F = F' + iF''$ is a complex factor with F' and F'' real constants over the frequency range of interest. Concerning only the non-resonant part, it follows for the total non-resonant intensity $I^{NR}_{CARS} \sim |E^{NR}_{CARS}|^2$ that

$$I^{NR}_{CARS} \sim e^{-1/2(\Delta\alpha + \alpha_c)L_S}(I_G + I_S + I_{MIX}) \quad (B5)$$

where the intensities from the glass I_G, sample I_S and interference term I_{MIX} are given by

$$I_G = \chi_G{}^2 L_G{}^2\,\text{sinc}^2(\phi_G)\{\cosh(\delta) + \cos[2(\phi_G + \phi_S)]\} \quad (B6)$$

$$I_S = \tfrac{1}{2}|F|^2\chi_G{}^2 L_S{}^2\left[\frac{\sinh^2(\delta/2) + \sin^2(\phi_S)}{(\delta/2)^2 + \phi_S{}^2}\right] \quad (B7)$$

$$I_{MIX} = \frac{\chi_G{}^2 L_G L_S\,\text{sinc}(\phi_G)}{\delta^2 + 4\phi_S{}^2} \times [X\cos(\phi_G)\sinh(\delta) - Y\sin(\phi_G)\cosh(\delta) + Y\sin(\phi_G + 2\phi_S)] \quad (B8)$$

with $\delta = \alpha L_S$, $X = -F'\delta + F'2\phi_S$ and $Y = F'2\phi_S + F''\delta$.

In Eqn (B7) we recognize, apart from the facto $\exp[-(\Delta\alpha + \alpha_c)L_S]$, the usual single-layer intensity expression in case of an absorbing sample.

In the absence of absorption (i.e. $\alpha_{c,p,s} = 0$, $F'' = 0$), Eqn. (B5) reduces to

$$I_{CARS}^{NR}(\delta = 0) \sim \chi_G{}^2 L_S{}^2 \operatorname{sinc}^2(\phi_S) \times \left[F' + 2 \frac{L_G}{L_S} \frac{\operatorname{sinc}(\phi_G)}{\operatorname{sinc}(\phi_S)} \cos(\phi_G + \phi_S) \right]^2 \quad \text{(B9)}$$

and the non-resonant background intensity is cancelled if

$$F' + 2 \frac{L_G}{L_S} \frac{\operatorname{sinc}(\phi_G)}{\operatorname{sinc}(\phi_S)} \cos(\phi_G + \phi_S) = 0 \quad \text{(B10)}$$

This condition can be fulfilled by proper selection of the lengths L_G and L_S and phase-mismatch factors ϕ_G and ϕ_S.

In case of absorption but under the condition $2\alpha_p + \alpha_s = \alpha_c$ ($\Delta\alpha = 0$), the imaginary part F'' still remains, which cannot be compensated for by phase mismatching. Since the phase mismatch $\Delta\beta$ in the phase-mismatch factors ϕ depends on the crossing angle η between the pump and Stokes beams, non-resonant background-free spectra can be obtained experimentally by varying the crossing angles at each wavenumber shift in the spectrum such that Eqn (B10) is fulfilled. In practice these angles are found from systematic minimum intensity searches by crossing angle–signal collection angle scans at various positions in the spectrum.